An alternative route to extract nickel and cobalt from non-commercial laterite ore

http://dx.doi.org/10.1590/0370-44672021750048

Pedro Paulo Medeiros Ribeiro[1,5]
https://orcid.org/0000-0002-1033-6275
Reiner Neumann[2,6]
https://orcid.org/0000-0002-6261-7140
Iranildes Daniel dos Santos[3,7]
https://orcid.org/0000-0001-5493-1079
Achilles Junqueira Bourdot Dutra[4,8]
https://orcid.org/0000-0001-8187-7186

[1]Universidade Federal do Rio de Janeiro - UFRJ,
Departamento e Programa de Engenharia
Metalúrgica e de Materiais/Poli/COPPE,
Rio de Janeiro – Rio de Janeiro - Brasil.

[2]Centro de Tecnologia Mineral - CETEM,
Serviço de Caracterização Tecnológica,
Rio de Janeiro – Rio de Janeiro - Brasil.

[3]Instituto Tecnológico Vale - ITV,
Ouro Preto - Minas Gerais - Brasil,
Belo Horizonte – Minas Gerais - Brasil.

[4]Universidade Federal do Rio de Janeiro – UFRJ,
Programa de Engenharia Metalúrgica e
de Materiais - COPPE,
Rio de Janeiro – Rio de Janeiro - Brasil.

E-mails: [5]ppmedeirosribeiro@metalmat.ufrj.br,
[6]reiner.neumann@gmail.com, [7]iranildes.santos@itv.org,
[8]adutra@metalmat.ufrj.br

Abstract

Laterite ores, which represent around two-thirds of nickel reserves, became an important source of nickel and cobalt metals. The objective of the present study was to investigate the efficiency of a hybrid route to extract nickel and cobalt present in a laterite ore sample which was not commercially attractive to be processed through the current routes. The process efficiency was investigated through the application of different test conditions, such as roast temperature, ore sample comminution, and moisture. Chemical analysis by atomic absorption was used to quantify the metals. The solid phase's identification and characterization were accomplished by X-ray diffraction and Scanning Electron Microscopy. The Rietveld Method was used for the mineral's phase quantification. In terms of nickel and cobalt extractions, the most favorable condition was: particle size smaller than 38 µm, 50% sulfuric acid (wt.%), and 10% moisture (wt.%), which permitted nickel, cobalt, magnesium, and iron recoveries of 84.5%, 92.0%, and 93.0%, 27.0% respectively. These results indicate the successful application of the route. In addition, it was found that chlorite, chromite, hematite, and goethite were identified as the main nickel and cobalt carriers present in the process residue.

Keywords: laterite, nickel, cobalt, residue, recovery, carriers.

1. Introduction

Nickel can be found in sulfide and laterite ores (Meshram, Abhilash, and Pandey 2018; Zhai *et al*. 2010). Most of the nickel extracted comes from sulfide ores (pentlandites). However, these reserves were extensively exploited and are depleting. Therefore, it is necessary to extract nickel from laterite ores (Oxley and Barcza 2013). Cobalt is another metal of high aggregated value that can be extracted together with nickel in the laterite ores (Senanayake *et al*. 2011; MacCarthy *et al*. 2016; G. H. Li *et al*. 2010).

The hybrid route named as the sulfation - roasting - leaching process is one of the most promising processes for the extraction of nickel and cobalt from laterite ores. It allows not only the nickel but also the cobalt recovery when compared to pyrometallurgical processes like the Rotary Kiln-Electric Arc Smelting (Keskinkilic 2019) in which cobalt is lost to the slag. If the comparison is made with hydrometallurgical processes, the sulfation-roasting-leaching process presents lower Capital and Operational Expenditure than processes using high pressure acid leaching. The acid consumption is considerably smaller than processes involving atmospheric leaching, such as heap and agitation leaching, even for hydrometallurgical processes using other leaching agents, such as chloride and carboxylic acids (McDonald and Whittington 2008). These processes demand more resistant digestors due to corrosion or expensive organic carbon sources and they also cannot be applied to all kinds of laterite ores (McDonald and Whittington 2008).

The main characteristic of the sulfation-roasting-leaching is the small amount of acid consumption which is in the range from 250 kg/t to 500 kg/t (X. Guo *et al*. 2009; D. Li *et al*. 2010). Nickel and cobalt recoveries can reach the range of 80-88%, 84-93%, respectively (D. Li *et al*. 2010; J. Li *et al*. 2009; Swamy, Kar, and Mohanty 2000; X. Guo *et al*. 2009). This type of process, although presenting a significant number of variables, such as roasting time and temperature, the number of heat-treatment steps, leaching temperature and time, agitation, solid/liquid ratio, and others, can be applied to all groups of nickel laterite ores and is easily operated (X. Guo *et al*. 2009).

The sulfation-roasting-leaching process consists of the following main steps: sulfation with sulfuric acid, heat treatments, and water leaching. After these steps, the liquor rich in nickel, cobalt, and magnesium is separated from the solid fraction containing insoluble compounds, such as those containing iron and aluminum, which are in the solid-state as hematite (Fe_2O_3) and alumina (Al_2O_3) or aluminum hydroxide ($Al(OH)_3$) by filtration. Then, nickel, cobalt, and magnesium will remain in the pregnant leaching solution (PLS) (Zhou *et al*. 2017; Zhang and Forssberg 1997; Oxley and Barcza 2013). The PLS is processed to recover nickel, cobalt, and magnesium separately through solvent extraction, ionic exchange, precipitation, electrowinning, and other techniques (Wang and Lee 2017).

Among all the existent variables in the sulfation-roasting-leaching process, the amount of water added before sulfation (moisture), the roasting temperature, and comminution directly affect the nickel and cobalt extraction in laterite ore (Basturkcu, Acarkan, and Gock 2017; Kolta and Askar 1975; Goss 1987; Swamy, Kar, and Mohanty 2003; Bunjaku, Kekkonen, and Holappa 2010). Moisture before sulfation makes it easier to mix sulfuric acid with the ore sample and also increases the porosity during the roasting steps, making the metals more reactive. Roasting temperature and comminution accelerate the kinetics of nickel and cobalt sulfates formation and increase the structural disorder of the mineral phases.

In many articles, investigation of the main influent variables in the different processes for nickel and cobalt extraction has been reported (Büyükakinci and Topkaya 2009; Kursunoglu, Ichlas, and Kaya 2017; Kursunoglu and Kaya 2016; Basturkcu, Acarkan, and Gock 2017; Swamy, Kar, and Mohanty 2000; X. Y. Guo *et al*. 2011; Liu *et al*. 2010). However, these works, especially those related to the sulfation-roasting-leaching process (X. Guo *et al*. 2009; Basturkcu and Acarkan 2016; D. Li *et al*. 2010; J. Li *et al*. 2009; Swamy, Kar, and Mohanty 2003, 2000), had the analysis of the variables of the employed processes as the main focus, without presenting explanations on the metal losses in the solid leaching residues, which is an important factor to improve metal recovery.

This way, the objective of the present study was to investigate the sulfation-roasting-leaching process efficiency applied to a lateritic ore sample from northern Brazil, which could not be processed through commercial routes due to its characteristics, such as high magnesium and iron contents. The effects caused due to changes in roasting temperature, comminution degree, and moisture modification were investigated. To achieve the goals, mineral phases were quantified for each step or condition applied. Finally, the behavior of nickel and cobalt throughout the processing was investigated and the best conditions to increase the recovery of these metals were proposed.

2. Materials and methods

2.1 Sample

The laterite ore sample came from the northern region of Brazil. Initially, the head sample, weighing 5 kg, was quartered using a Jones riffle sampler to obtain 1 kg-samples. In the sequence, the samples were homogenized in humid conditions and taken to an oven at 80 °C for 24 hours. Through the conical heap method, samples of approximately 10 g were separated for the tests.

2.2 Selective sulfation procedure

Initially, 10 g of the ore sample were mixed with 1 to 4 g of distilled water plus 5 g of sulfuric acid. After this step (sulfation), the samples were pre-heated to 265 °C (pre-roasting) with a heating rate of 10°C/min in a muffle furnace. The samples were kept at this temperature for 60 minutes. Then the samples were cooled to room temperature in a moisture-free atmosphere, and later de-agglomerated and weighted. In the next stage, they were taken back to the furnace and subjected to a heat treatment at 680±3, 740±3, 780±3, 800±2, or 830±2°C for 20min. The heating rate for all the experiments was 10°C/min. The temperature range from 680 to 830 °C was chosen because this is the region where ferric sulfate decomposes and nickel-cobalt sulfates are stable (680°C) and the region where also nickel-cobalt sulfates decompose (830°C). The pre-roasting temperature, time, and roasting time were defined in a previous study (Ribeiro *et al*. 2021). For the roasting temperature of 680°C, two other variables

were investigated: water content before sulfation (moisture) and the effect of milling up to 100% below 38 µm. The comminution was done with an agate mortar & pestle set. After the roasting step, the samples were cooled to room temperature. Each test was repeated three times to confirm reproducibility.

The leaching was carried out at a temperature of 80 °C for 30 min. Each experiment consisted of a mixture of 10 g of the processed ore plus 80 g of distilled water. The mechanical stirring speed was 300 rpm. These conditions were established according to previous studies (Ribeiro *et al*. 2019). The metal recovery was calculated according to Eq. (1) where C_i is the concentration (mg/L) of the metal i in the PLS measured by atomic absorption, t_i is the percentage of metal *i* (wt.%) in the solid leaching residue, V_{Ci} is the volume measured for the PLS (L), and m_{Ti} is the solid leaching residue mass (mg). The flowchart of Figure 1 summarizes the steps of the sulfation-roasting-leaching process and each route used according to the variables chosen. Pearson's correlation coefficient (*r*) between the metal recovery and the roasting temperature or the phase content was calculated according to Eq. (2) (Carr and Bossu 2014). Where x_i is the roasting temperature of the i^{th} test, $\bar{x}$ is the average roasting temperature used in the tests (from the 1^{st} to the n^{th} test), y_i is the recovery of each metal for test *i* or the mineral phase content, and $\bar{y}$ the average of the metal recoveries for all tests or the average mineral phase content formed at different roasting temperatures.

$$recovery = \frac{C_i V_{ci}}{\left(\frac{t_i m_{ti}}{100} + C_i V_{ci} \right)} \times 100 \qquad (1)$$

$$r = \frac{\sum_{i=1}^{n}(x_i - \bar{x})(y_i - \bar{y})}{\sqrt{\sum_{i=1}^{n}(x_i - \bar{x})^2 \sum_{i=1}^{n}(y_i - \bar{y})^2}} \qquad (2)$$

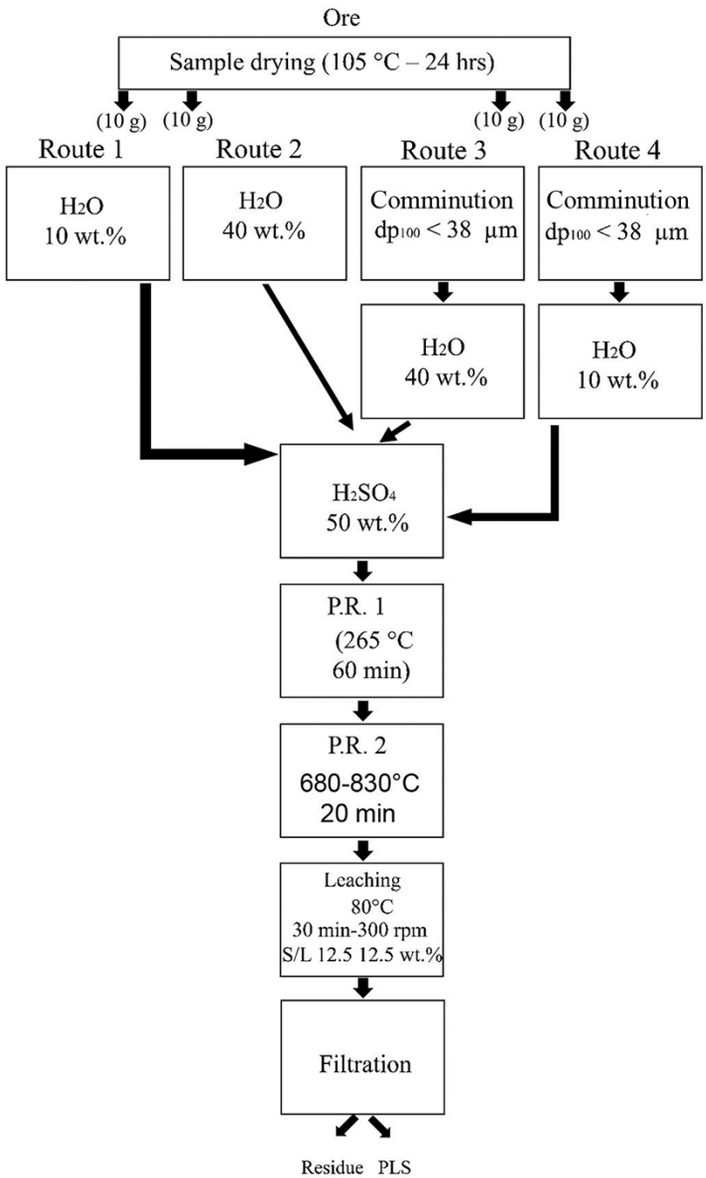

Figure 1 - Flowchart of the sulfation-roasting-leaching process used to extract nickel and cobalt from laterite ore for four different conditions. P.R. 1: pre-roasting; P.R. 2: roasting; S/L: solid/liquid ratio.

2.3 Mineralogical characterization of ore and leaching residue

The X-ray diffraction analysis was carried out in a Bruker-AXS D4 Endeavor diffractometer, with Co k_α radiation (λ = 1.78897 Å), Fe k_β filter, and a Lynx Eye position sensitive detector (PSD). The diffraction angles (2θ) were scanned from 4 to 105°. A Bruker-AXS's DIFFRAC.EVA suite software and PDF4 plus ICDD databases were used for the identification of the minerals. The Rietveld refinement was done with a Bruker-AXS's Topas 5.0 software and the crystal structure data for the minerals from the Bruker Structure Database. The internal standard method was used to quantify the amorphous phase amounts with fluorite as the spike phase.

The images were captured with a Scanning Electron Microscope (SEM) FEI Quanta 400 - coupled to a Bruker Quantax 800 Energy Dispersive X-Ray Spectroscopy (EDS) system and an X-Flash 5010 detector.

The chemical composition of the ore sample was determined by x-ray fluorescence and/or atomic absorption. It presented a nickel (NiO), cobalt (Co_3O_4), magnesium (MgO), and iron (Fe_2O_3) oxides contents (wt.%) of 1.9, 0.2, 7.8, and 36.9, respectively. The X-ray diffraction analysis revealed the presence of actinolite (1.0%), quartz (26.4%), goethite (27.0%), chromite (8.0), lizardite (3.4%), hematite (10.0%), chlorite (18.5%), chrysotile (0.5%), talc (3.7%) and magnetite (1.4%) as the main crystalline phases in the sample. The average chemical composition of each of the main minerals, previously found by the X-ray diffraction, was determined by EDS and recalculated to include the water content of the mineral. The mineralogical nature of the phases identified in the solid leaching residues was considered to be the same as the fresh ore phases (only the content of each phase was recalculated), since there was no substantial change in the mineralogical composition of those phases in the solid leaching residues. The exceptions were for hematite, goethite, and chromite whose average compositions, including the impurities in the solid leaching residues, were also recalculated.

3. Results

3.1 Sample characterization

The nickel and cobalt distributions in each of the main carrier minerals in the ore sample are presented in Table 1. It can be observed that the main nickel carrier is chlorite (73.6 wt.%), while hematite was the main cobalt carrier (25.0 wt.%). Asbolane, identified only by SEM, is also an important cobalt carrier, but due to its low crystallinity, it could not be identified by XRD or even quantified, appearing as other minerals in Table 1.

Table 1 - Nickel and cobalt distribution by mineral.

Distribution (wt.%)/Phase	Ni	Co
Actinolite	0.1	0
Goethite	19.4	8.1
Cromite	0.2	12.0
Lizardite	5.4	0.0
Hematite	0.2	25.0
Chlorite	73.6	9.2
Chrysotile	1.1	
Others	0.0	45.7

The analytical data on the partition for Mg, Ni, Fe, Co is shown in Table 2. The greatest nickel amount is concentrated in the size fraction smaller than 106 µm, while cobalt is concentrated in both the coarser (26.80 wt.%) and finer (36.00 wt%). Cobalt is also evenly distributed between the particle size range from 601 to 150 µm. To reduce the losses of nickel and cobalt, the head sample was used instead of the fraction size.

Table 2 - Analytical data for each size distribution (in wt.%) for Mg, Ni, Fe, Co.

Size distribution	Mg	Ni	Fe	Co	Ni Partition	Co Partition
d < 106µm	3.07	2.09	37.49	0.09	53.39	36.00
106 < d < 150µm	3.13	1.74	28.48	0.09	7.97	6.46
150 < d < 213µm	3.1	1.6	26.18	0.1	6.18	6.04
213 < d < 301µm	3.53	1.65	26.45	0.11	5.73	5.98
301 < d < 425µm	4	1.72	26.83	0.11	6.11	6.12
425 < d < 601µm	4.33	1.77	26.41	0.11	5.50	5.36
601 < d < 850µm	4.67	1.74	24.69	0.13	6.18	7.24
d > 850µm	4.6	1.2	15.37	0.23	8.93	26.80
Head	3.1	1.72	29.3	0.09	100.00	100.00

3.2 Sulfation, pre-roasting, and roasting of the ore sample - route 1

For the sulfation, 10 g of the ore sample was mixed to 1 g of water plus 5 g of sulfuric acid, making a total of 16 g. After this step, the samples were submitted to a pre-roasting step. The mass mean and standard deviation after this step was 14.1 g and 0.16 g, respectively. Assuming that the water added was evaporated before pre-roasting, the mass loss observed should be associated with the unreacted goethite dihydroxylation (Eq. 3) (Gualtieri and Venturelli 1999), ferric sulfate formation (Eq. (4)), and partial decomposition of the ferric sulfate according to Eq. (5) (no thermodynamic data was found in the HSC database), which is important due to the increase of SO_3 concentration at the vicinity of the mineral structure, allowing the sulfation of other metals, such as nickel and cobalt (Basturkcu and Acarkan 2016). After the sulfation step, the pug was composed basically of ferric and ferrous sulfates and quartz, as indicated by X-ray diffraction of the dried samples.

$$2FeO(OH)_{(s)} \rightarrow Fe_2O_{3(s)} + H_2O_{(g)};\ \Delta G^0_{265°C} = -27{,}07\ kJ \quad (3)$$

$$3H_2SO_4 + Fe_2O_3 \rightarrow Fe_2(SO_4)_3 + 3H_2O(g);\ \Delta G^0_{25°C} = -163{,}02\ kJ \quad (4)$$

$$Fe_2(SO_4)_{3(s)} + H_2O_{(g)} \rightarrow 2Fe(OH)SO_{4(s)} + SO_{3(g)} \quad (5)$$

The Ni, Co, Fe, and Mg recoveries by route 1 as a function of roasting temperature can be observed in Table 3. It can be noted that nickel recovery varied moderately with the increase in temperature. The highest nickel recovery was achieved at 740 °C (85.7%). Nickel recovery showed a downward trend for temperatures higher than 740 °C. This drop can be attributed to the loss of stability of nickel sulfate with increasing temperatures. The thermal decomposition of nickel sulfate starts at a temperature around 675 °C, in the air under atmospheric pressure (Kolta and Askar 1975). Pearson's correlation coefficient calculated for the relationship between nickel recovery and the roasting temperature was -0.32. This result indicates that there is a weak negative influence of temperature. This negative effect of temperature on nickel recovery would have been reversed if the highest temperature considered was 780°C. In this scenario, Pearson's correlation coefficient would be 0.62. The change observed in the temperature effect was due to the SO_3, which loses its stability as the roasting temperature rises, being converted to SO_2 and O_2 according to Eq. (6). Considering the total system pressure equal to 1 atm and oxygen pressure equal to 0.21 atm the ratio P_{SO3}/P_{SO2} decreases from 0.45 to 0.36 when the roasting temperature is increased from 780°C to 800°C.

Table 3 - Ni, Co, Fe, and Mg recoveries as a function of roasting temperature according to route 1. Where r is the Pearson's correlation coefficient and σ the standard deviation for each metal recovery. Conditions: H_2SO_4: 50 wt.%; H_2O: 10 wt.%; pre-roasting temperature and time: 265 °C, 60 min; roasting time: 20 min; Leaching temperature, time, solid/liquid ratio, and stirring speed: 80 °C, 30 min, 12.5% 400 rpm.

Temperature (°C)	Ni	Co	Fe	Mg
680	73.49	73.72	27.06	71.37
740	85.68	74.83	16.58	84.88
760	79.45	74.65	12.64	79.52
780	80.59	93.27	5.49	74.40
800	72.45	84.63	2.13	75.04
830	70.05	85.51	1.28	88.33
Mean	77.64	82.58	7.62	80.43
σ	5.93	7.94	9.95	6.59
r	-0.32	0.68	-0.98	0.52

$$2SO_{2(g)} + O_{2(g)} \rightarrow 2SO_{3(g)};\ \Delta G^0_T = -197.13 + 0.19T\ kJ \quad (from\ 200°C\ to\ 1000°C) \quad (6)$$

Iron, however, showed a very strong Pearson's correlation coefficient (-0.98) and its recovery decreased with the temperature increase from 27.1% at 680 °C to 1.3% at 830 °C. This decrease in iron recovery can be attributed to increasing the instability of the existing ferric sulfate. The higher the test temperature, the higher the degree of conversion of sulfate to oxide for the same roasting time. Thermogravimetric analysis results from literature indicated that the thermal decomposition temperature of the ferric sulfate in the air starts around 575 °C (Kolta and Askar 1975). About 68% of the cobalt recovery increase (r = 0.68) is influenced by the roasting temperature change. Cobalt sulfate is stabler than nickel sulfate. Data from literature reported that the thermal decomposition temperature of cobalt sulfate in the air starts around 720 °C (Kolta and Askar 1975). The fact that cobalt recovery increased even at temperatures higher than 720 °C (780°C was the temperature which rendered the highest cobalt recovery, 93.3%) may be associated with other variables such as the higher decomposition degree of ferric sulfate. The temperature increase allows the release of more sulfur oxides, increasing the probability of contact between cobalt oxide with the gas, which converts it to sulfate. Furnace limitations may have also caused this behavior, since the layer sample in the used muffle furnace was static, demanding more time for the

whole sample bed thickness to achieve the desired temperature. Another contribution to this phenomenon can be related to the increase of the partial pressure of gases (SO_2/SO_3) from the decomposition of trivalent sulfates (Basturkcu and Acarkan 2016). This increase of the partial pressure turns the reaction of metal sulfate conversion to oxide (Eq. (7) more difficult. Magnesium recovery was around 71.4% at 680 °C and increased to 88.3% at 830 °C. Pearson's correlation coefficient between magnesium recovery, and the temperature was 0.52. The magnesium sulfate formed is very stable and does not decompose in the temperature range investigated. Data from literature indicated that the magnesium sulfate decomposition starts around 900 °C (Tagawa 1984). Besides, the increase of this metal recovery might be caused by the same reasons as those described for cobalt.

$$M_2(SO_4)_{3(s)} \rightarrow M_2O_{3(s)} + 3SO_{3(g)} \quad (7)$$

3.3 Chemical and mineralogical characterization of solid leaching residue – route 1

The characterization of the solid leaching residues aimed at investigating the nickel and cobalt contents in the solid residue and which minerals they were associated with. In Figure 2, it is possible to identify the main crystalline phases present in the solid leaching residues of each sample. The identified phases were: hematite, quartz, chlorite, goethite, and chromite in all the samples. It can be observed that the increase of roasting temperature leads to a decrease in the intensity of some peak phases, such as chlorite and goethite, and the growth of others, such as hematite and quartz. Figure 3 shows the micrographs obtained by SEM/EDS, indicating the presence of the main minerals found in Figure 2. It can be noted in Figure 3 that the average size of the quartz and hematite particles are smaller than those of the other phases present, and the hematite particles have a certain amount of impurities, such as Al_2O_3 and SiO_2, as detected by EDS (not shown in Figure 3).

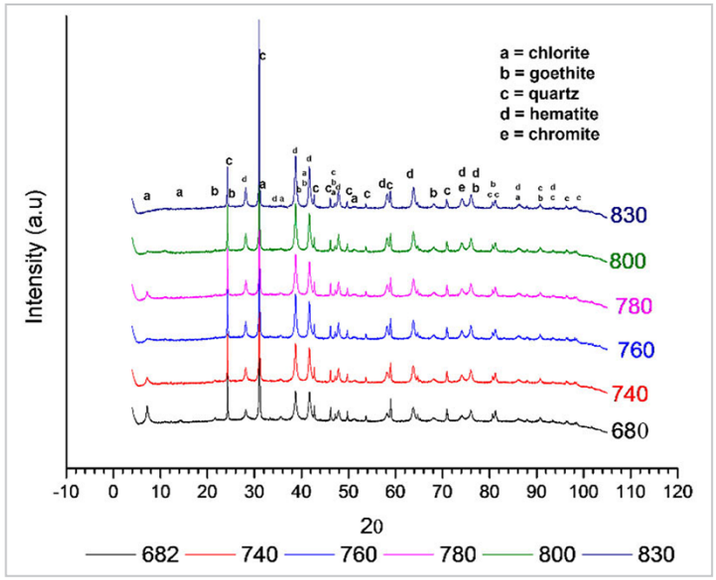

Figure 2 - XRD patterns of solid leaching residue for different roasting temperatures.

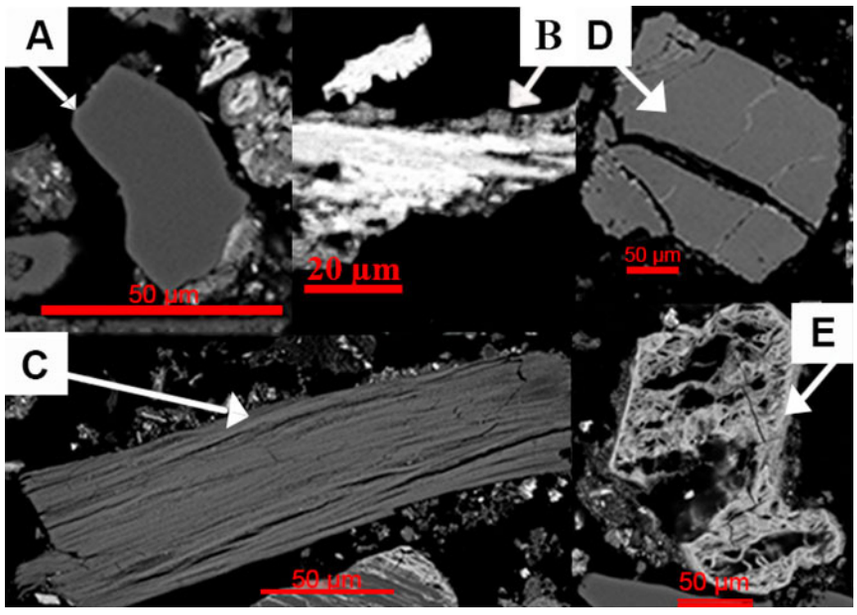

Figure 3 - The typical aspect of the main minerals found in solid leaching residue for the temperatures of 680 °C, 740 °C, 780 °C, 800 °C, and 830 °C. A = quartz, B = hematite, C = chlorite, D = chromite e E = goethite.

The mineral phase quantification of the residue for each roasting temperature tested was accomplished with the help of the Rietveld method. The mathematical parameters R_{wp} (equivalent mass-weighted residue) and GOF (goodness of fit parameter), which indicate the quality of the refinement, were in the range of 2.5-1.39 and 1.96-1.95, respectively. These values are indicative of a good quality of refinement. The results are further ensured by the conciliation of the calculated chemical composition derived from XRD and Rietveld refinement against the chemical analysis for each temperature, graphically represented in Figure 4. The average difference between the iron content (in the form of oxide - Fe_2O_3) calculated by the Rietveld method and that obtained by the chemical analysis was 2%. Silicon dioxide, not appearing in the graph of Figure 4 because it was not quantified by chemical analysis but by X-ray diffraction only.

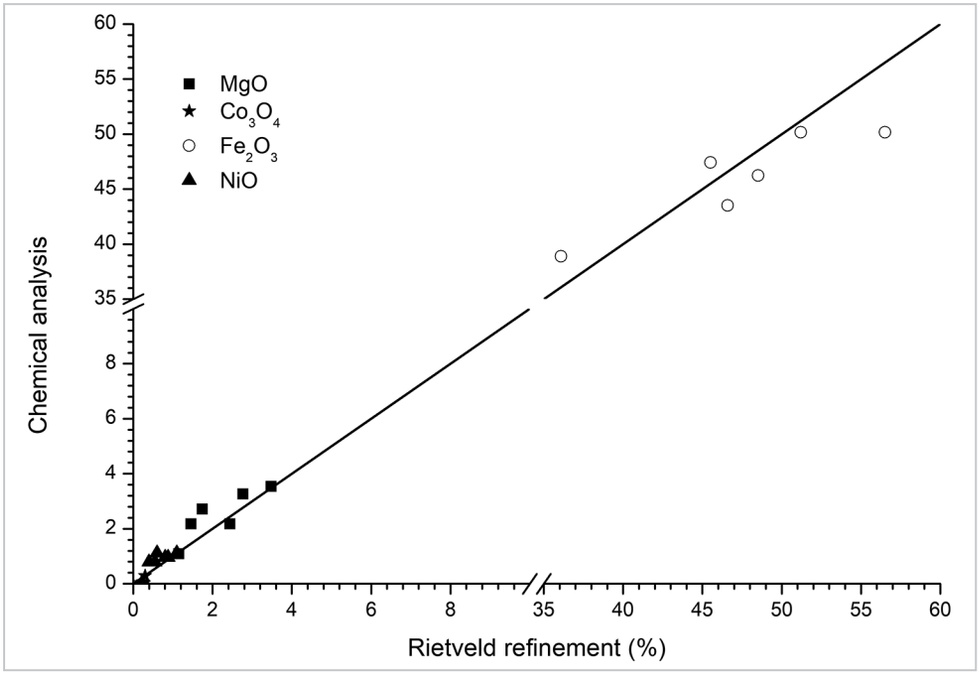

Figure 4 - Conciliation of the chemical composition calculated from phases quantification by XRD/Rietveld against the chemical analysis by atomic absorption – route 1.

Results of the refinement for the solid leaching residues are shown in Figure 5. It is possible to note that the chromite content remained almost constant for all the roasting temperatures investigated. Quartz and hematite are the main minerals found in the solid leaching residue and the hematite content in the residue increased significantly compared to the content found in the raw ore sample.

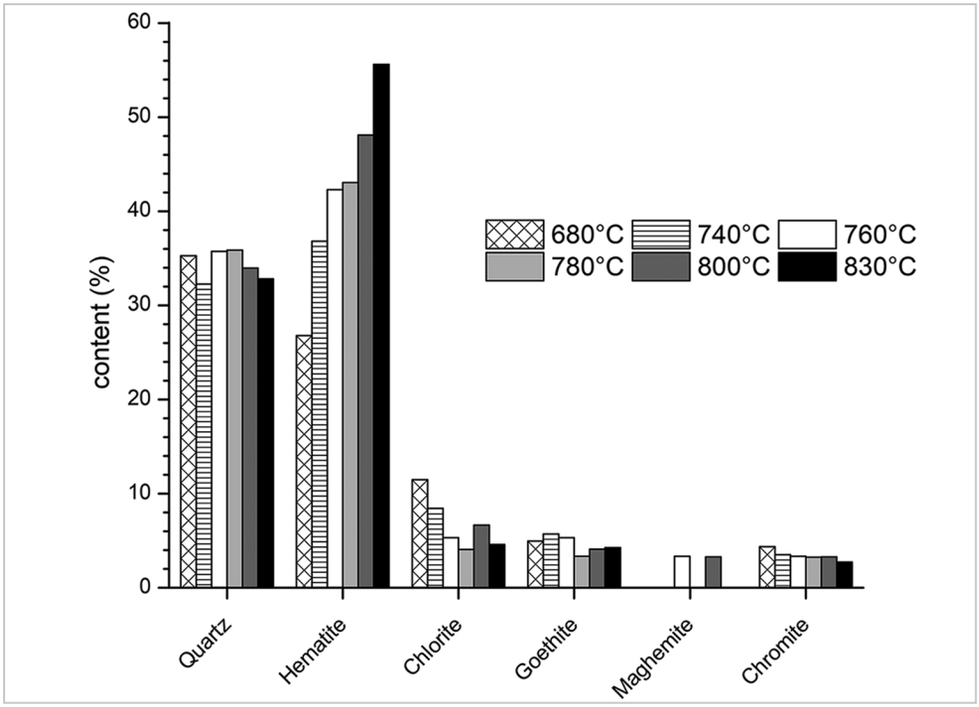

Figure 5 - Results of phases quantification by the Rietveld method for different roasting temperatures – Route 1.

The increase of the hematite content in the solid leaching residues, as shown in Figure 5, is possibly due to the reactions of Equations (8) and (9). The ferric sulfate formed from the iron, present in the ore sample as goethite or hematite, undergoes thermal decomposition with the increase of temperature, being converted to Fe_2O_3. This fact justifies the increase of the hematite content in the solid leaching residues. The higher the roasting temperature, the higher the conversion rate. Therefore, the hematite content in the solid leaching residues notably increased with the increase of test temperature, raising from 32% (wt.%) to 56% (wt.%) with the increase of roasting temperature from 680 °C to 830 °C. The quartz content did not show a correlation with temperature, remaining practically constant. The reactions of chlorite and lizardite minerals with sulfuric acid leads to the formation of SiO_2 and $MgSO_4$ according to equations (10) and (11). However, the quartz oxide produced is an amorphous phase while the magnesium oxide is crystalline. The chlorite content present in the solid leaching residue ranged from 13.9% (wt.%) to 4.6% (wt.%) for the highest and the lowest roasting temperatures, 680 °C and 830 °C respectively. The existence of chlorite and goethite after the heat treatment above their decomposition temperatures is explained in (Ribeiro *et al.* 2020). Pearson's correlation coefficient calculated for the chlorite content in the solid leaching residue as a function of temperature was -0.81, indicating a negative correlation between the two variables. An increase in the roasting temperature affects the stability of chlorite, according to Eq. (12), which shows the chlorite decomposition reaction. The increase in temperature leads to product formation (SiO_2, H_2O, MgO, and Al_2O_3), as proven by the variation of Gibbs free energy at 1 atm pressure with temperature for the reaction of Eq. (12) calculated with the aid of the HSC software. The Gibbs' free energy decreased with the increase of temperature.

$$1/3Fe_2(SO_4)_{3(s)} \rightarrow 1/3Fe_2O_{3(s)} + SO_{3(g)} \quad \Delta G^0_{800°C} = -5.30 \text{ kJ} \tag{8}$$

$$2Fe(OH)SO_{4(s)} \rightarrow Fe_2O_{3(s)} + H_2O_{(g)} + 2SO_{3(g)} \tag{9}$$

$$Mg_5Al_2Si_3O_{10}(OH)_8 + 8H_2SO_4 \rightarrow 5MgSO_4 + Al_2(SO_4)_3 + 3SiO_2 + 12H_2O(g) \quad \Delta G^0_{25°C} = -380{,}11 \text{ kJ} \tag{10}$$

$$Mg_3Si_2O5(OH)_4 + 3H_2SO_4 \rightarrow 3MgSO_4 + 2SiO_2 + 5H_2O \quad \Delta G^0_{25°C} = -195{,}12 \text{ kJ} \tag{11}$$

$$Mg_5Al_2Si_3O_{10}(OH)_8 \rightarrow 3SiO_2 + 4H_2O_{(g)} + 5MgO + Al_2O_3 \quad \Delta G^0_T = 347.41 - 0.59T \text{ kJ} \tag{12}$$

The nickel and cobalt distribution (wt.%) among minerals present in the solid leaching residue as a function of roasting temperature is shown in Figure 6. It can be observed that most of the remaining nickel was found in chlorite (around 82.4% at 680°C). However, the nickel amount carried by hematite becomes important as the roasting temperature is increased to 830°C, achieving 32.3%. The increase in nickel content in hematite can be explained by the formation of hematite from goethite and sulfate decompositions, leading to new crystalized hematite with different compositions from the one identified in the raw ore. Hematite was also the most important iron and cobalt carriers in the solid leaching residue. The cobalt percent lost in this phase changed from 36.7% to 64.9% when the roasting temperature was increased from 680°C to 830 °C, respectively. Amorphous silica could be another source of nickel and cobalt losses. However, no amorphous phase was detected in the solid leaching residue after the quantification using the internal standard method. Almost all the magnesium in the solid leaching residue was found in chlorite.

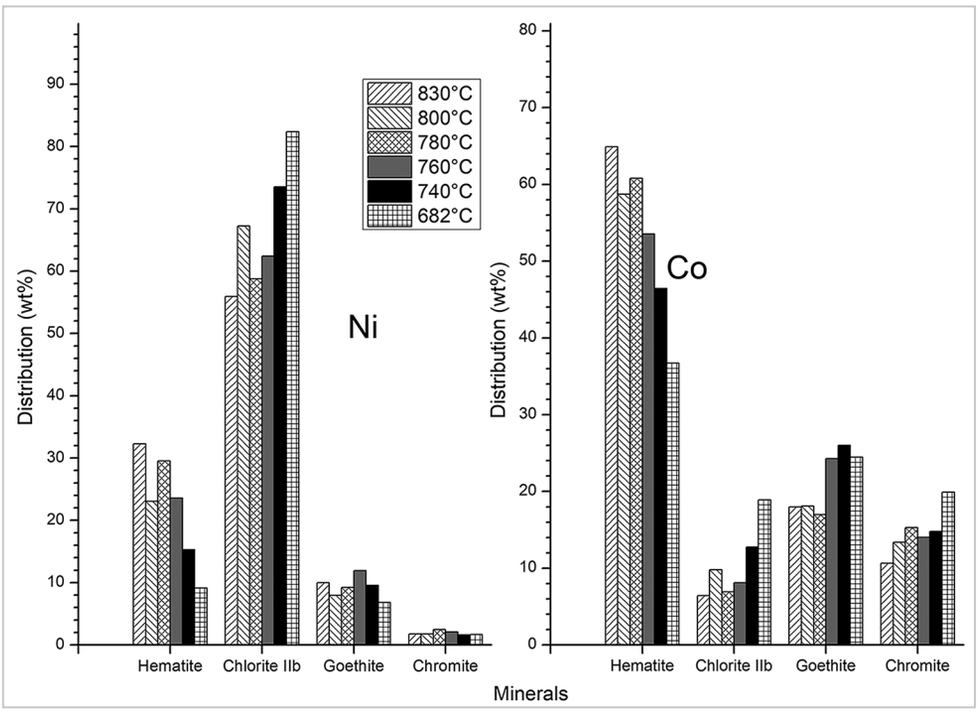

Figure 6 - Nickel and cobalt distribution by mineral present in solid leaching residue for each roasting temperature – Route 1.

A SEM micrograph of a chlorite particle partially attacked by sulfuric acid is shown in Figure 7. EDS analyses identified nickel in the regions with light grayscale (point 1), but this metal was not found in the darker ones (point 2). The sampling aspect changed from a tabular shape to a lamellar one after the sulfuric acid attack. The changes were due to a phase transformation in which the reaction of chlorite with sulfuric acid gives quartz and sulfates as products (Eq. (10)). Bivalent sulfates, such as nickel and magnesium sulfates, are soluble in water and are entrained by the aqueous leaching solution. However, trivalent sulfates, such as iron and aluminum sulfates, present low water solubility and precipitate in the form of oxides and hydroxides in the same place. The chlorite particle, with an average particle size of 226 µm, is practically intact in the central region and wholly attacked in the peripheral region. In terms of surface area, it is possible to emphasize that sulfuric acid did not attack about one-third of the particle. The particle size reduction of the ore samples can contribute positively to the increase of nickel extraction, since it can decrease the unreacted mineral amount. The presence of carbon and chlorine in the sample is due to the epoxy resin in which it was embedded before analyses.

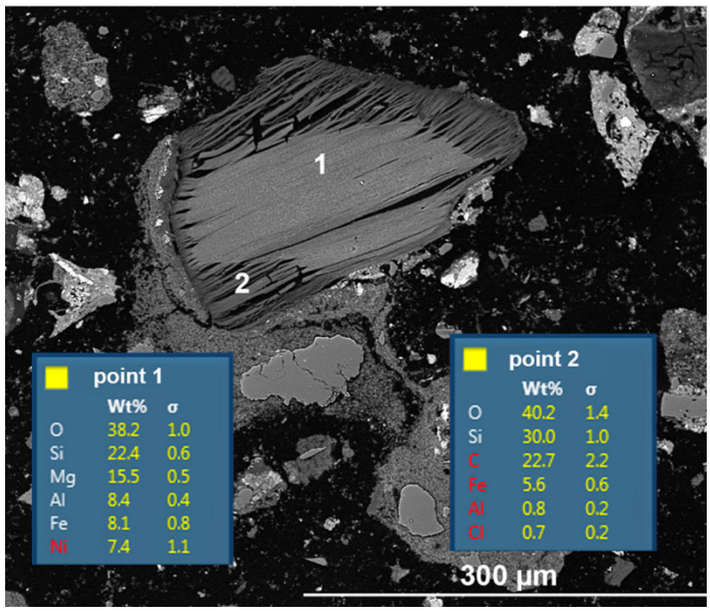

Figure 7 - SEM micrograph of a chlorite particle partially reacted with sulfuric acid after leaching according to route 1.

As shown previously herein, most of the remaining nickel in solid leaching residues was found in chlorite. New tests were conducted aiming at improving the process efficiency. In these tests, the roasting temperature was set at 680 °C. This roasting temperature was chosen because of the higher amount of metal sulfate found in the samples after the heat-treatment, allowing a better investigation of other variables in the process efficiency, and also to obtain a higher reactivity of the sulfur gas SO_3. The ferric sulfate stability is smaller than the other ones, such as nickel, cobalt, and magnesium sulfates, and decreases with increasing temperatures. At 680°C, Gibbs' free energy for the reactions (8), (13), (14), and (15) are respectively 16.30, 52.69, 77.36, and 88.23 kJ.

3.4 Sulfation, pre-roasting, and roasting of the ore sample – routes 2, 3, and 4

To improve nickel and cobalt recoveries, some modifications to the process had to be implemented.The focus of the changes was to investigate whether similar or even higher nickel and cobalt recoveries could be obtained at lower roasting temperatures with changes in other variables. The first change was to increase the water content added previously to sulfation from 10% to 40% (Route 2).The second change consisted of adding 40% moisture (water) in the ore sample comminuted up to 100% smaller than 38 µm (Route 3) and the third change was done by the ore sample comminution up to 100% smaller than 38 µm and adding 10% moisture (Route 4). The obtained results are presented in Figure 8. The increase of the added water content (Route 2) led to an increase in nickel and cobalt recovery from 73.49 and 73.72% to 81.2 and 89.1%, respectively. Iron and magnesium also had changes in their recoveries. Both increased from 27.1% to 38.3 and 71.4% to 88.5%, respectively. The increase of the water content before leaching makes the acid-ore mixture more effective during sulfation and also creates porous particles during roasting (Ribeiro *et al.* 2020). These combinations tend to increase the metal's recovery. However, it is important to mention that the addition of 40% moisture is efficient in the muffle furnace, but it creates operational problems if the furnace chosen for the thermal treatment is the rotary kiln. In this type of furnace, the pug (a mixture of ore, acid, and water) agglomerates and compromises the product flow after the thermal treatments.

Particle size reduction to 100% below 38 µm (routes 3 and 4) resulted in an even more significant increase in nickel, cobalt, and magnesium extractions. The recoveries of nickel, cobalt, and magnesium rose to 86.0%, 93.7%, and 94.0%, while the iron extraction was 25.5%, for route 3. The sample processed according to route 4 extracted 84.5%, 92.0%, 27.0%, and 93.0% of nickel, cobalt, iron, and magnesium, respectively. It produced slightly smaller values for nickel and cobalt when compared to route 3 and this was due to the reduction in moisture. Particle size

reduction leads to an increase in the solid structural disorder (Basturkcu, Acarkan, and Gock 2017) which can lead to physicochemical changes, such as oxidation and decomposition. These changes may be consequences of the mechanical activation of the sample due to grinding. Besides, it leads to an increase in the surface area of the sample (new surfaces not previously attacked by the reagent) which makes the probability of reagent-solid contact higher. These results corroborate with those found by (Basturkcu, Acarkan, and Gock 2017).

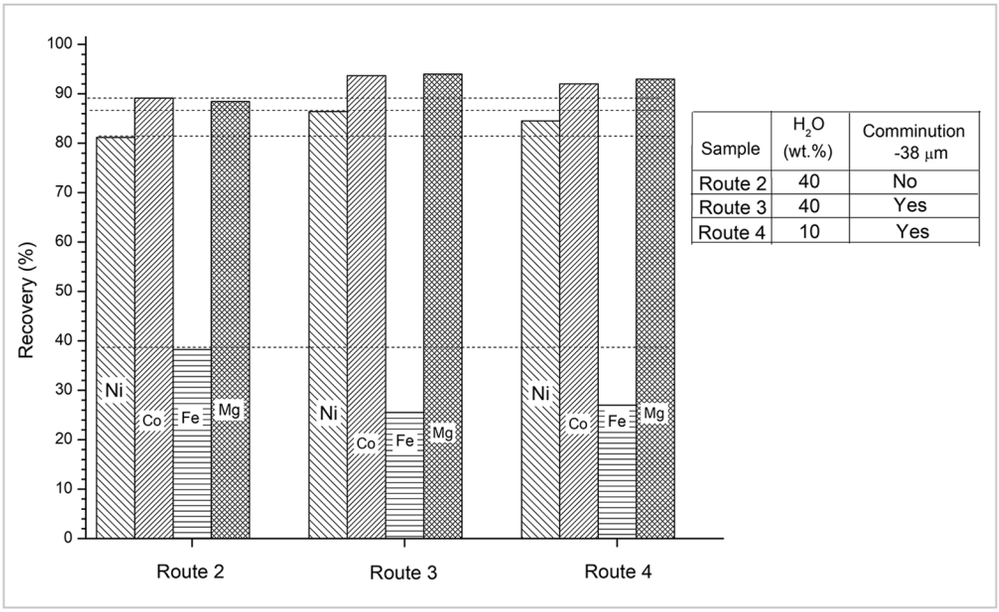

Figure 8 - Nickel, cobalt, iron, and magnesium recoveries from the raw ore sample after applying the sulfation-roasting-leaching process for routes 2, 3, and 4.

$$NiSO_{4(s)} \rightarrow NiO(s) + SO_{3(g)} \quad \Delta G_{680°C} = 52.69\ kJ \qquad (13)$$

$$CoSO_{4(s)} \rightarrow CoO_{(s)} + SO_{3(g)} \quad \Delta G_{680°C} = 77.36\ kJ \qquad (14)$$

$$MgSO_{4(s)} \rightarrow MgO_{(s)} + SO_{3(g)} \quad \Delta G_{680°C} = 88.23\ kJ \qquad (15)$$

3.5 Chemical and mineralogical characterization of solid leaching residue – routes 2, 3, and 4

The phase quantification by the Rietveld method of the solid leaching residues of laterite ore samples processed according to routes 1, 2, 3, and 4, is shown in Fig. 9. In the modifications, concerning the results of Fig. 5, for the roasting temperature of 680 °C, the chlorite content in solid leaching residues decreased significantly, dropping from 13.9 wt.% to 6.1 wt.% for the route 2, and 5.0 wt.% for route 3. For the sample processed through route 4, the recovery was slightly smaller when compared to the one processed through route 2. As previously described, moisture favors the sulfation of metal oxides present in ore samples, which contributes to the increase of the reactivity of several minerals with acid, as in the chlorite case. However, the goethite content in the solid leaching residues decreased only in the comminuted samples, from 6.0 wt.% to 3.8 wt.% for route 4, for example. The higher amount of goethite in the sample processed through route 2 can be explained by equations (3) and (16). In these equations, there can be observed that an increase of the partial pressure of water vapor ($H_2O_{(v)}$) shifts the reaction equilibrium to the left side. More details about the influence of the gases partial pressure in the reactions can be found in (Ribeiro *et al.* 2019). This behavior helps to explain why the moisture increase leads to an increase in the goethite content present in the sample processed through route 2.

$$2FeOOH_{(s)} + 3H_2SO_4(l)) \rightarrow Fe_2(SO_4)_{3(s)} + 4H_2O_{(g)} \quad \Delta G^0_{25°C} = -115.94\ kJ \qquad (16)$$

The conciliation of the chemical composition calculated from the quantification of phases by the XRD/Rietveld method against chemical analysis can be observed in Figure 10. A divergence is observed between the iron contents calculated by the two methods. Assuming that the chemical analysis is correct, this error might be associated with the overestimation of hematite by XRD. The mathematical parameters R_{wp} and GOF were 3.13 - 3.2 (route 1), 2.41 -2.45 (route 2), 3.4 - 3.1 (route 3), and 4.2 –2.8 (route 4).

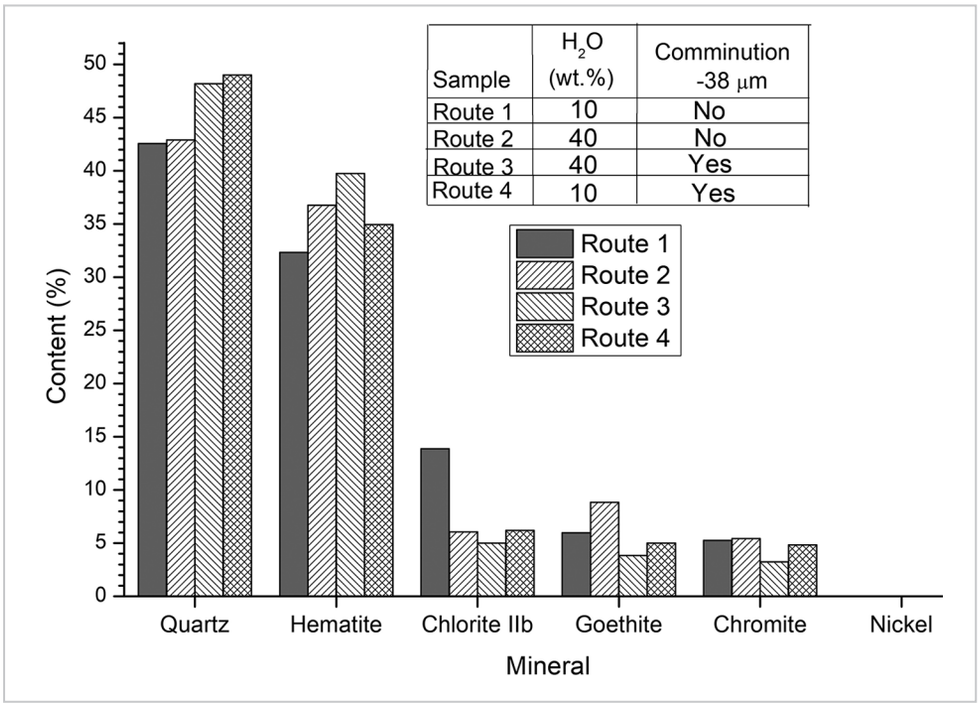

Figure 9 - Phase quantification by Rietveld method of solid leaching residues of laterite ore samples processed according routes 1, 2, 3, and 4.

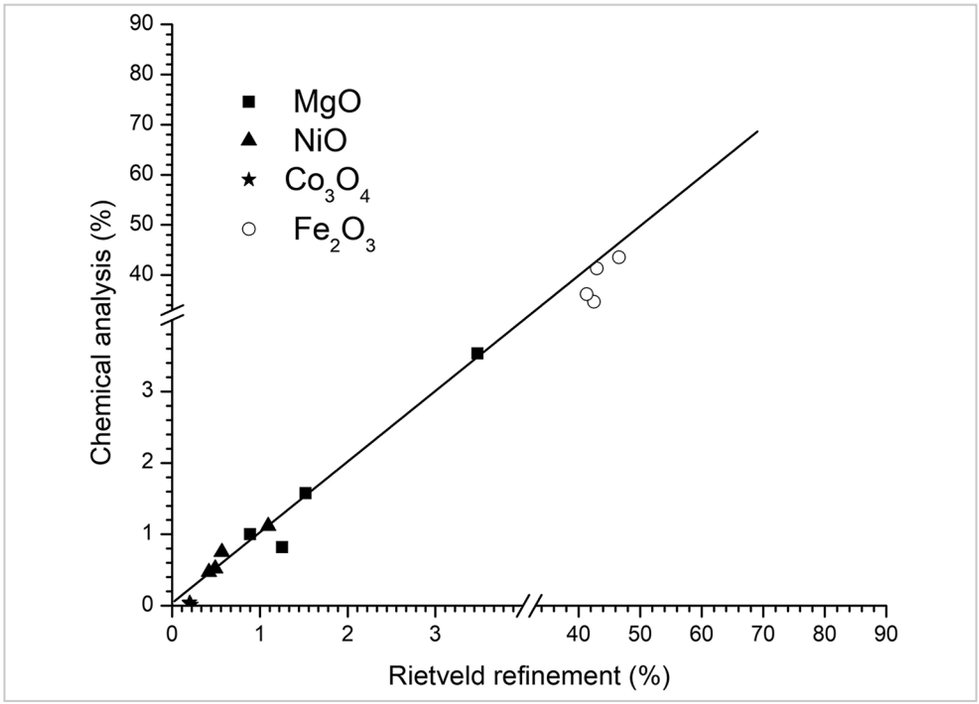

Figure 10 - Conciliation of the chemical composition calculated from phases quantification by XRD/ Rietveld against the chemical analysis of solid leaching residues for the laterite ore samples processed according to routes 1, 2, 3, and 4.

The nickel and cobalt distributions by mineral in the solid leaching residue for the sample processed according to each route are presented in Figure 11. It can be observed that the main nickel carrier was chlorite and the percent of nickel lost in this phase increased from 57.3% in the sample processed through route 4 to 82.3% in the sample processed through route 1. These results can be explained by the increase in structural disorder of chlorite due to comminution. Hematite was also an important nickel carrier, being responsible for 24.3% of the sample processed through route 3. The most important cobalt carrier once again was hematite. In this phase, the cobalt losses varied from 35.9% in the sample processed through route 4 to 50.4% in the sample processed through route 3. Goethite, chromite, and chlorite were also responsible for cobalt losses in the solid leaching residues. In the sample processed through route 4, more than 40% of the cobalt losses were in goethite, while for the sample processed through route 1, both chlorite and chromite were important cobalt carriers. The cobalt fraction in the chromite phase varied from 15% in the sample processed through route 4 to 20% in the sample processed through route 1, besides this, iron predominated in hematite, while the main magnesium carrier was chlorite.

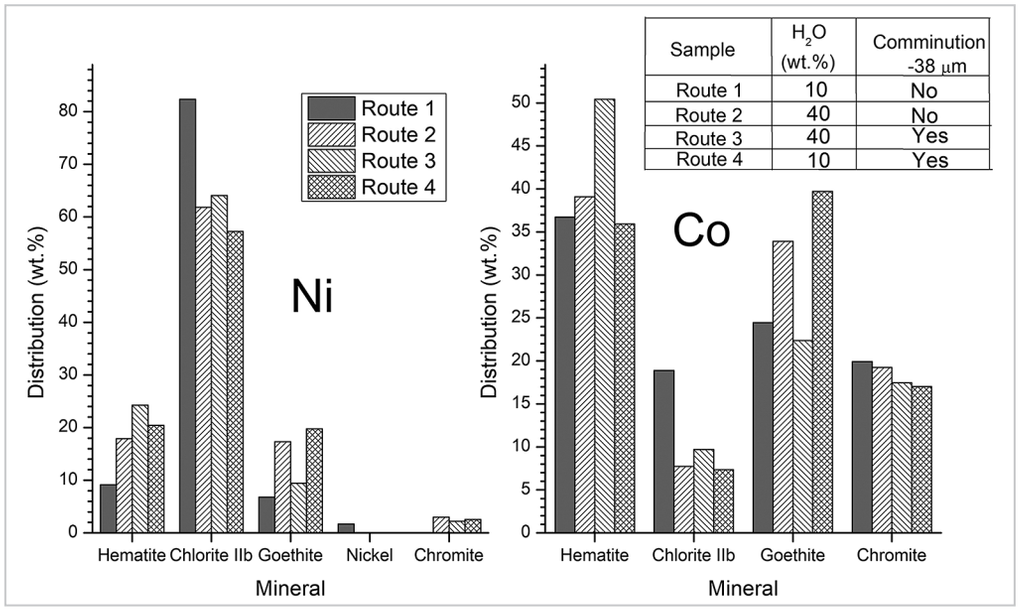

Figure 11 - Nickel and cobalt distribution by mineral in the solid leaching residue for each route applied.

Figure 11. Nickel and cobalt distribution by mineral in the solid leaching residue for each route applied.

The four different routes investigated showed that it is possible to recover nickel and cobalt from non-commercial laterite ore. Roasting temperature, moisture, and particle size changes have a significant impact on the recovery and stability of the main nickel and cobalt carriers in the solid leaching residues. In terms of nickel and cobalt extractions, the most favorable route was route 3. However, this option has two critical points: the need for comminution and the high amount of water added. In terms of iron removal, the most advantageous conditions were obtained by route 1. Even though the drop in nickel recovery from 86.4% to 80.5% and the need for higher roasting temperature (780 °C), the amount of water added was smaller and the comminution of the ore sample was not necessary. The choice between these options depends on the focus of the processing. However, processing samples with 40% moisture might be difficult, this way, leading to the choice of the ones with 10% moisture.

4. Conclusions

The sulfation-roasting leaching process is promising to extract nickel and cobalt from laterite ore. It can be used to recover nickel and cobalt from a kind of laterite ore which, otherwise, would be considered worthless material. However, many variables can affect the efficiency of the hybrid route. Among them, roasting temperature, moisture, and particle size changes have a significant impact on the stability of the main nickel and cobalt carriers in the solid leaching residues. The best results were obtained for the roasting temperatures of 680 °C and 780 °C. At the roasting temperature of 780 °C; with the addition of 10% moisture (wt.%); and 50% of sulfuric acid, nickel, and cobalt recoveries were 80.5% and 93.2%. At the roasting temperature of 680 °C; the addition of 10 wt.% moisture; comminution up to 38 μm; and 50 wt.% sulfuric acid (route 4), the nickel and cobalt recoveries were 84.5%, 92.0%, respectively. The iron extracted from routes 1 and 4 were 5.5% and 27.0%, respectively.

The quantitative phase analysis by the XRD/Rietveld method indicated that quartz, hematite, chlorite, and goethite were the main minerals present in the solid leaching residue. In terms of nickel and cobalt carriers, however, the main ones are chlorite, hematite, chromite, and goethite. Their metals (Ni and Co) contents change according to the process variables, which are determinants for an efficient nickel and cobalt recovery.

References

BASTURKCU, H.; ACARKAN, N. Separation of nickel and iron from lateritic ore using a digestion – roasting – leaching – precipitation process. ***Physicochemical Problems of Mineral Processing***, v. 52, n. 2, p. 564–574, 2016.

BASTURKCU, H.; ACARKAN, N.; GOCK, E. The role of mechanical activation on atmospheric leaching of a lateritic nickel ore. ***International Journal of Mineral Processing***, v. 163, p. 1–8, 2017.

BUNJAKU, A.; KEKKONEN, M.; HOLAPPA, L. Phenomena in thermal treatment of lateritic nickel ores up to 1300oC. *In*: INTERNATIONAL FERROALLOYS CONGRESS, 12., 2010, Helsinki, Finland. ***Proceedings*** **[...].** [*S. l.: s. n.*], 2010. p. 641–652. (Other Ferroalloys Fundamentals).

BÜYÜKAKINCI, E.; TOPKAYA, Y. A. Extraction of nickel from lateritic ores at atmospheric pressure with agitation leaching. ***Hydrometallurgy***, v. 97, n. 1-2, p. 33–38, 2009.

CARR, P.; BOSSU, S. ***Advanced equity derivatives:*** volatility and correlation. New York: Wiley, 2014. 176p.

GOSS, C. J. The kinetics and reaction mechanism of the goethite to hematite transformation. ***Mineralogical Magazine***,

v. 51, n. 361, p. 437–451, 1987.
GUALTIERI, A. F.; VENTURELLI, P. In situ study of the goethite-hematite phase transformation by real time synchotron powder diffraction. ***American Mineralogist***, v. 84, p. 895–904, 1999.
GUO, X.; LI, D.; PARK, K. H.; TIAN, Q.; WU, Z. Leaching behavior of metals from a limonitic nickel laterite using a sulfation-roasting-leaching process. ***Hydrometallurgy***, v. 99, n. 3-4, p. 144–150, 2009.
GUO, X. Y.; SHI, W. T.; LI, D.;TIAN, Q. Leaching behavior of metals from limonitic laterite ore by high pressure acid leaching. ***Transactions of Nonferrous Metals Society of China***, v. 21, n. 1, p. 191–195, 2011.
KESKINKILIC, E. Nickel laterite smelting processes and some examples of recent possible modifications to the conventional route. ***Metals***, v. 9, n. 9, 2019.
KOLTA, G. A.; ASKAR, M. H. Thermal decomposition of some metal sulphates. ***Thermochimica Acta***, v.11, n. 1, p. 65-72, 1975.
KURSUNOGLU, S.; ICHLAS, Z. T.; KAYA, M. Leaching method selection for Caldag lateritic nickel ore by the analytic hierarchy process (AHP). ***Hydrometallurgy***, v. 171, p. 179–184, 2017.
KURSUNOGLU, S.; KAYA, M. Atmospheric pressure acid leaching of Caldag lateritic nickel ore. ***International Journal of Mineral Processing***, v. 150, p. 1–8, 2016.
LI, D.; PARK, K. H.; WU, Z.; GUO, X. Y. Response surface design for nickel recovery from laterite by sulfation--roasting-leaching process. ***Transactions of Nonferrous Metals Society of China***, v. 20, p. s92–s9 , 2010a.
LI, G. H.; RAO, M. J.; LI, Q.; PENG, Z. Extraction of cobalt from laterite ores by citric acid in presence of ammonium bifluoride. ***Transactions of Nonferrous Metals Society of China***, v. 20, p. 1517–1520, 2010b.
LI, J.; LI, X.; HU, Q.; WANG, Z. Effect of pre-roasting on leaching of laterite. ***Hydrometallurgy***, v. 99, n. 1-2, p. 84–88, 2009.
LIU, W. R.; LI, X. H.; HU, Q. Y.; WANG, Z. X.; GU, K. Z.; LI, J. H.; ZHANG, L. X. Pretreatment study on chloridizing segregation and magnetic separation of low-grade nickel laterites. ***Transactions of Nonferrous Metals Society of China***, v. 20, p. s82–s86, 2010.
MACCARTHY, J.; NOSRATI, A.; SKINNER, W.; ADDAI-MENSAH, J. Atmospheric acid leaching mechanisms and kinetics and rheological studies of a low grade saprolitic nickel laterite ore. ***Hydrometallurgy***, v. 160, p. 26–37, 2016.
MCDONALD, R. G.; WHITTINGTON, B. I. Atmospheric acid leaching of nickel laterites review. Part II. Chloride and bio-technologies. ***Hydrometallurgy***, v. 91, n. 1-4, p. 56–69, 2008.
MESHRAM, P.; ABHILASH; PANDEY, B. D. Advanced Review on Extraction of Nickel from Primary and Secondary Sources. ***Mineral Processing and Extractive Metallurgy Review***, v. 40, n. 3, p. 157–193, 2018.
OXLEY, A.; BARCZA, N. Hydro-pyro integration in the processing of nickel laterites. ***Minerals Engineering***, v. 54, p. 2–13, 2013.
RIBEIRO, P. P. M.; NEUMANN, R.; SANTOS, I. D.; REZENDE, M. C.; RADINO-ROUSE, P.; DUTRA, A. J. B. Nickel carriers in laterite ores and their influence on the mechanism of nickel extraction by sulfation-roasting--leaching process. ***Minerals Engineering***, v. 131, p. 90–97, 2019.
RIBEIRO, P. P. M.; SOUZA, L. C. M.; NEUMANN, R.; SANTOS, I. D.; DUTRA, A. J. B. Nickel and cobalt losses from laterite ore after the sulfation-roasting-leaching processing. ***Journal of Materials Research and Technology***, v. 9, n. 6, p. 12404–12415, 2020.
SENANAYAKE, G.; CHILDS, J.; AKERSTROM, B. D.; PUGAEV, D. Reductive acid leaching of laterite and metal oxides - A review with new data for Fe(Ni,Co)OOH and a limonitic ore. ***Hydrometallurgy***, v. 110, n. 1, p. 13–32, 2011.
SWAMY, Y. V.; KAR, B. B.; MOHANTY, J. K. Physico-chemical characterization and sulphatization roasting of low-grade nickeliferous laterites. ***Hydrometallurgy***, v. 69, n. 1-3, p. 89–98, 2003.
SWAMY, Y. V; KAR, B. B.; MOHANTY, J. K. Some aspects of nickel extraction from chromitiferous overburden by sulphatization roasting. ***Minerals Engineering***, v. 13, n. 14-15, p. 14-15, 2000.
TAGAWA, H. Thermal decomposition temperatures of metals sulfates. ***Thermochimica Acta***, v. 80, p. 23–33, 2000, 1984.
WANG, L.Y.; LEE, M. S. Separation of Co(II) and Ni(II) from chloride leach solution of nickel laterite ore by solvent extraction with Cyanex 301. ***International Journal of Mineral Processing***, v. 166, p. 45–52, 2017.
ZHAI, X. J.; WU, Q.; FU, Y.; MA, L. Z.; FAN, C. L; LI, N. J. Leaching of nickel laterite ore assisted by microwave technique. ***Transactions of Nonferrous Metals Society of China***, v. 20, p. s77–s81, 2010.
ZHANG, S.; FORSSBERG, E. Mechanical separation-oriented characterization of electronic scrap. Resources, Conservation and Recycling, v. 21, n. 4, p. 247–269, 1997.
ZHOU, S.; WEI, Y.; LI, B.; WANG, H.; MA, B.; WANG, C.; LUO, X. Mineralogical characterization and design of a treatment process for Yunnan nickel laterite ore, China. ***International Journal of Mineral Processing***, v. 159, p. 51–59, 2017.

Received: 6 July 2021 - Accepted: 15 March 2022.